Vacuum 177 (2020) 109376

Contents lists available at ScienceDirect

Vacuum

journal homepage: http://www.elsevier.com/locate/vacuum

Microstructure evolution of Cu-1.0Co-0.65Si-0.1Ti alloy during hot deformation

Yongfeng Geng [a,b,c,d], Xu Li [d], Yi Zhang [a,b,c,*], Yanlin Jia [e,**], Honglei Zhou [f], Baohong Tian [a,b,c], Yong Liu [a,b,c], Alex A. Volinsky [g], Xiaohui Zhang [a,b,c], Kexing Song [a,b,c], Ping Liu [f], Xiaohong Chen [f]

[a] School of Materials Science and Engineering, Henan University of Science and Technology, Luoyang 471023, PR China
[b] Provincial and Ministerial Co-construction of Collaborative Innovation Center for Non-ferrous Metal New Materials and Advanced Processing Technology, Henan Province, Luoyang 471023, PR China
[c] Henan Province Key Laboratory of Nonferrous Materials Science and Processing Technology, Luoyang 471023, PR China
[d] Center for Advanced Measurement Science, National Institute of Metrology, Beijing 100029, PR China
[e] College of Materials Science and Engineering, Beijing University of Technology, Beijing, 100124, PR China
[f] School of Materials Science and Engineering, Shanghai University of Technology, Shanghai 200000, PR China
[g] Department of Mechanical Engineering, University of South Florida, Tampa, 33620, USA

ARTICLE INFO

Keywords:
Cu-1.0Co-0.65Si-0.1Ti alloy
Hot compression
Flow stress
Microstructure evolution

ABSTRACT

The Cu-1.0Co-0.65Si-0.1Ti alloy was obtained by vacuum melting, and then the hot deformation experiment was carried out by using the Gleeble-1500 simulator at 0.001–10 s^{-1} strain rates and 500–900 °C deformation temperatures. The microstructure evolution of Cu-1.0Co-0.65Si-0.1Ti alloy was discussed. The micro texture of Cu-1.0Co-0.65Si-0.1Ti alloy was analyzed by EBSD. With the deformation temperature increasing from 700 to 800 °C, the dynamic recrystallization was promoted and the texture of Cu-1.0Co-0.65Si-0.1Ti alloy transformed from the {011} <100> Goss texture to the {112} <111> copper texture. The HAGBs and geometrically necessary dislocation (GND) density were calculated, respectively, which can also indicate that the increasing of temperature promoted the dynamic recrystallization. The critical strain for the initiation of dynamic recrystallization in Cu-Co-Si-Ti alloy deformed at 0.01 s^{-1},800 °C and 0.001 s^{-1},800 °C was 0.089 and 0.035, respectively. And it can be inferred that the increasing of deformation temperature or decreasing of strain rate can reduce the critical strain and promote the dynamic recrystallization. Finally, the precipitate was determined to be Co_2Si.

1. Introduction

Copper alloys are widely used as the lead frames, electrical and electronics industry, electric vacuum device and so on due to their combination of excellent conductivity and thermal conductivity, high corrosion resistance [1–8]. And electric vacuum device mainly includes high-frequency and ultra-high frequency emission tubes, waveguide tubes, magnetron tubes and so on, which need the high-purity oxygen free copper and dispersion strengthened oxygen free copper. Cu-Ni-Si, Cu-Cr, Cu-Ag and so on series alloys, which are mainly used as the lead frames and integrated circuits, have attracted the great interest of many researchers in recent years. However, with the fast development of equipment and technology, the higher performance requirements of copper alloys are required. Many researchers have investigated many methods to improve the comprehensive performance of copper alloys. But the most commonly methods to improve the properties of copper alloys is always the addition of trace alloy elements and rare earth elements in the copper matrix, such as Cr [9], Sn [10], Ag [11], Mg [6,12], Zr [13], Ti [14,15], Ce [12,16] and so on. Then according to the combination of the heat treatment and deformation, the high strength of the copper alloys with the nanoscale precipitates, which can meet the performance requirements of the industrial applications.

Li et al. [17] reported the aging behavior of the quaternary Cu-Ni-Co-Si alloy, and found that the alloy exhibited a high performance

* Corresponding author. School of Materials Science and Engineering, Henan University of Science and Technology, Luoyang, 471023, PR China
** Corresponding author.
E-mail addresses: yizhang@haust.edu.cn, zhshgu436@163.com (Y. Zhang), jiayanlin@126.com (Y. Jia).

https://doi.org/10.1016/j.vacuum.2020.109376
Received 10 March 2020; Received in revised form 29 March 2020; Accepted 3 April 2020
Available online 28 April 2020
0042-207X/© 2020 Elsevier Ltd. All rights reserved.

Table 1
The nominal and analyzed composition of Cu-1.0Co-0.65Si-0.1Ti alloy.

Alloy	Alloy element (wt.%)							
	Co	Si	Ti	C	H	O	N	Cu
Cu-1.0Co-0.65Si-0.1Ti	0.895	0.601	0.094	0.09	0.03	0.05	0.12	Bal.

with the dispersion strengthened nanoscale δ-(Ni, Co)$_2$Si precipitates. Huang et al. [18] obtained a high electrical conductivity and strength of Cu-Ni-Co-Si-Mg by the two-step heat treatment and found that the δ-(Co, Ni)$_2$Si precipitate was promoted due to the addition of Co. Zhang et al. [19] revealed the influence of Ti addition on the microstructure and properties of graphite flake/Cu-Ti composites fabricated by vacuum hot pressing, and found that the Ti addition showed a significant effect on the microstructure, strength and electrical conductivity. Zhao et al. [20] investigated a Cu-Ni-Sn alloy with the high strength and ductility, and the results showed that the nucleation of dynamic recrystallization was promoted due to the addition of Si and Ti. Moreover, many researchers investigated the performance of Cu-Ni-Si alloys through heat treatment and deformation [21,22,23]. Because researchers have done a lot of researches on Cu-Ni-Si system alloys, we want to use the Co element instead of Ni element to obtain the Cu-Co-Si alloy with the nanoscale

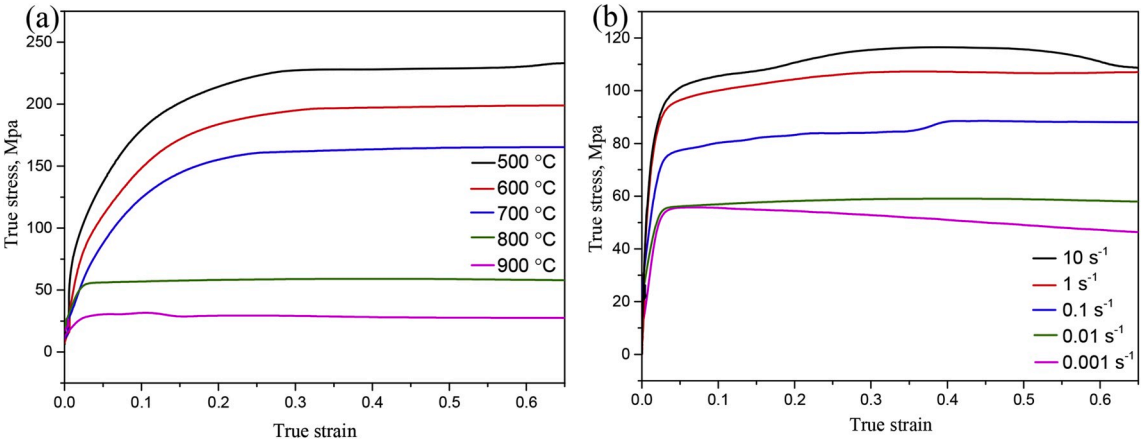

Fig. 1. True stress-True strain of Cu-1.0Co-0.65Si-0.1Ti alloy deformed at 0.01 s^{-1} (a) and 800 °C (b).

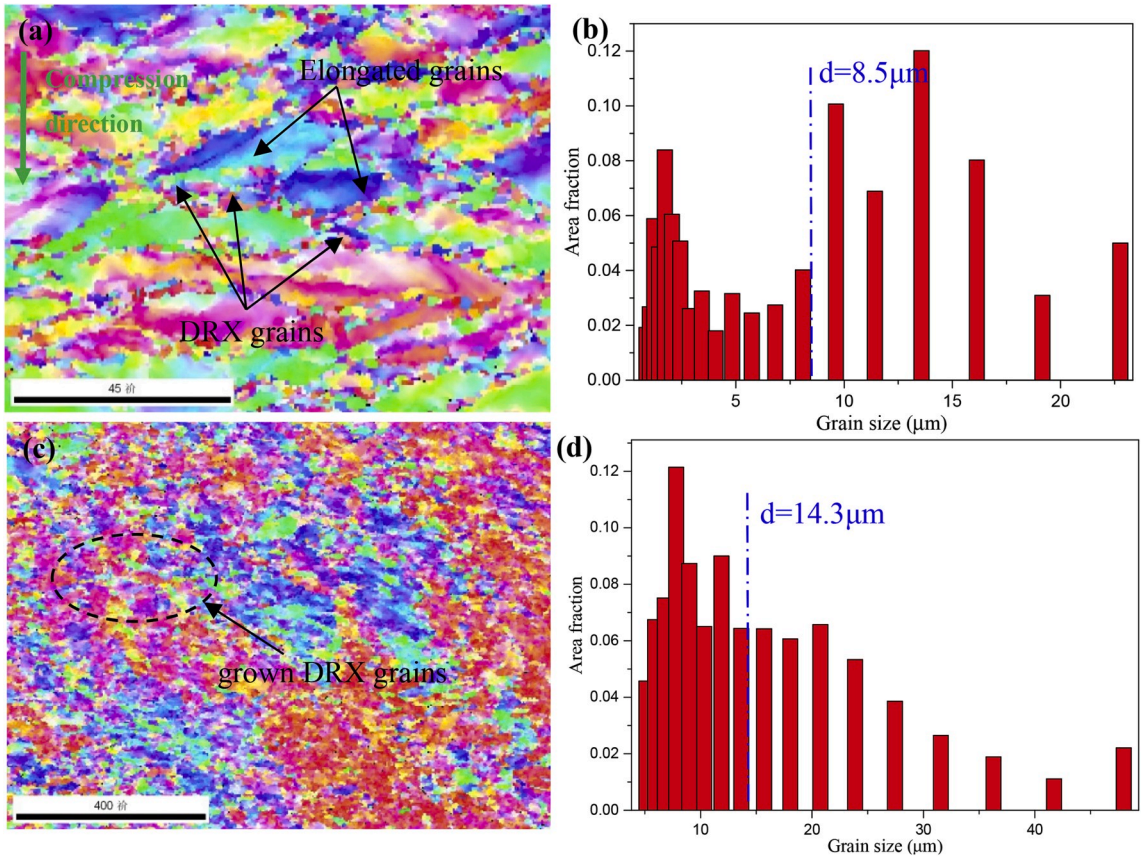

Fig. 2. EBSD images of Cu-1.0Co-0.65Si-0.1Ti alloy under different deformation conditions:(a) 700 °C and 0.01 s^{-1};(b) grain size distributions of (a); (c) 800 °C and 0.01 s^{-1};(d) grain size distributions of (c).

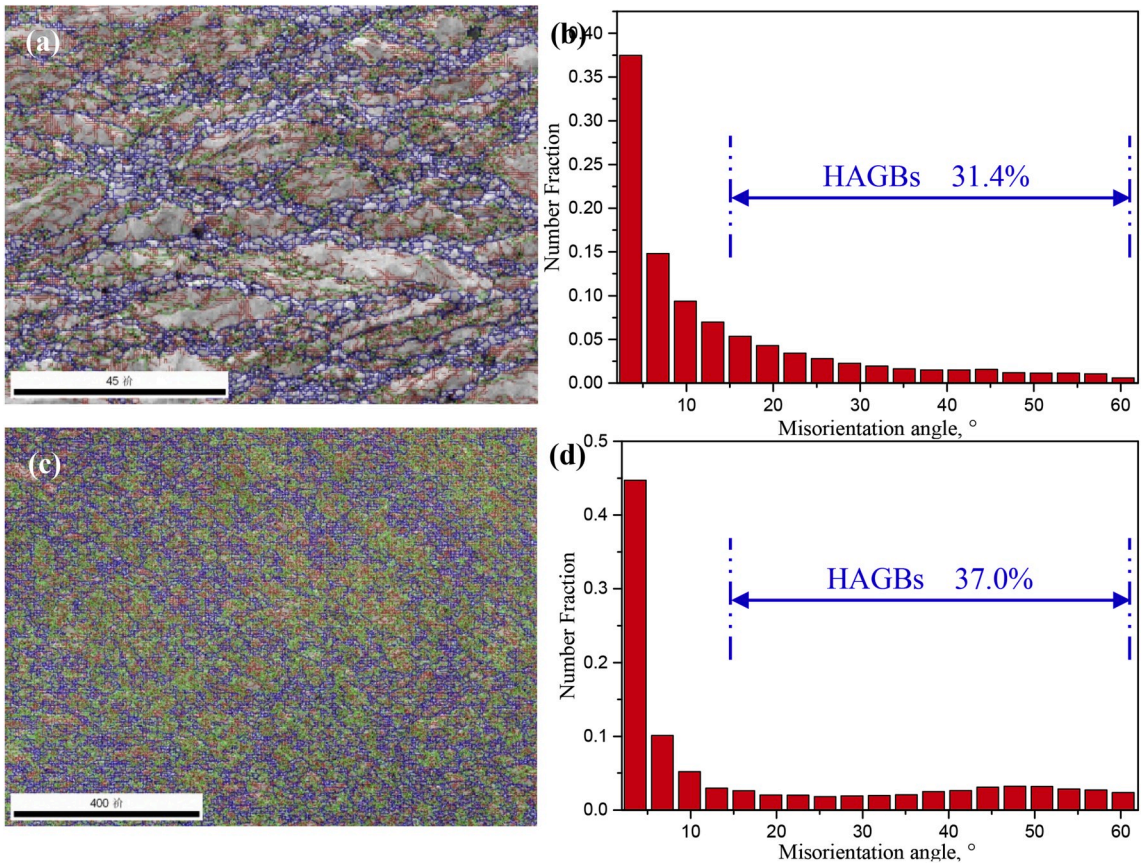

Fig. 3. EBSD orientation maps and misorientation angles distributions of Cu-1.0Co-0.65Si-0.1Ti alloy deformed at 0.01 s^{-1} and different temperatures: (a) and (b) deformed at 700 °C; (c) and (d) deformed at 800 °C.

Co_2Si precipitate. Based on the above researches, the copper alloy (Cu-1.0Co-0.65Si-0.1Ti) was obtained by the addition of Co, Si and Ti. Thus, the hot deformation behavior of the Cu-1.0Co-0.65Si-0.1Ti alloy with hot compression test was investigated in this paper.

2. Experimental materials and procedures

The Cu-1.0Co-0.65Si-0.1Ti alloy used in this experiment was obtained by the vacuum melting with the 99% standard electrolytic cathode copper, pure Co, Si and Cu-45% Ti master alloy in the ZG-0.01-40-4 vacuum medium frequency induction furnace. The nominal composition and actual composition of Cu-1.0Co-0.65Si-0.1Ti alloy are shown in Table .1. It can be seen that there is a certain difference between the nominal composition of the alloy and the actual tested composition, because the percent of Co, Si and Ti will cause partial loss in the melting process. In the melting process, a certain vacuum atmosphere was needed, i.e. the argon was introduced to prevent the alloy oxidation. The pouring temperature of the experiment was set between 1150 and 1250 °C, and the size of the crucible used for pouring is internal diameter of ~90 mm, ~20 mm thickness and ~190 mm height. After cooling to the room temperature and annealing at 960 °C for 1 h, the ingots were extruded into 30 mm diameter bars by the XJ-500 metal profile extrusion machine. Moreover, the samples also need the solution treatment at 960 °C for 1 h and then cut into Φ 8 mm × 12 mm cylinders by wire cutting before the hot compression tests, which were carried out at 500–900 °C temperature and 0.001–10 s^{-1} strain rates ranges, respectively, by the Gleeble-1500D thermo-mechanical simulator. As for the selection of hot deformation temperature, on one hand, the cracks tend to occur below 500 °C with high strain rates on the basis of practical production. And the hot deformation temperature of Cu-based alloy usually selected as 500–900 °C. On the other hand, according to the Cu-Co phase diagram in our previous paper [15], the phases at room temperature are Cu and ε-Co. Thus, the deformation temperature was selected as 500–900 °C and the strain rate was 0.001 s^1 to 10 s^1. It should be noted that the experiment conditions of high vacuum or sub vacuum are needed in the experiment in order to obtain the Cu-1.0Co-0.65Si-0.1Ti alloy. Firstly, from the beginning of alloy smelting, the furnace needs to be filled with argon all the time to ensure that oxygen will not enter the furnace to cause the alloy oxidation. Moreover, in the process of solid solution treatment of alloy in the heat treatment furnace, it is very important to inject the argon into the furnace to keep the vacuum state, because the alloy is easier to oxidize at high temperature, resulting in the structure defects and decreasing the performance of the alloy.

The microstructure evolution after hot deformation for the Cu-1.0Co-0.65Si-0.1Ti alloy was observed by the JSM-7800F backscatter scanning electron microscope and JEM-2100 transmission electron microscope (TEM). The samples for EBSD (electron backscatter diffraction) observations were obtained by the mechanical polishing and electropolishing, and then observed by the backscatter scanning electron microscope. The samples for TEM observations with a size of 3 mm diameter and 50 μm thickness were ion thinned by the Gatan 691 ion thinner. Especially, for the EBSD and TEM observations by the JSM-7800F backscatter scanning electron microscope and JEM-2100 transmission electron microscope, a higher vacuum is required to prevent the contamination of the specimens.

3. Results

3.1. Flow stress

Fig. 1 shows the true stress-true strain curves of Cu-1.0Co-0.65Si-

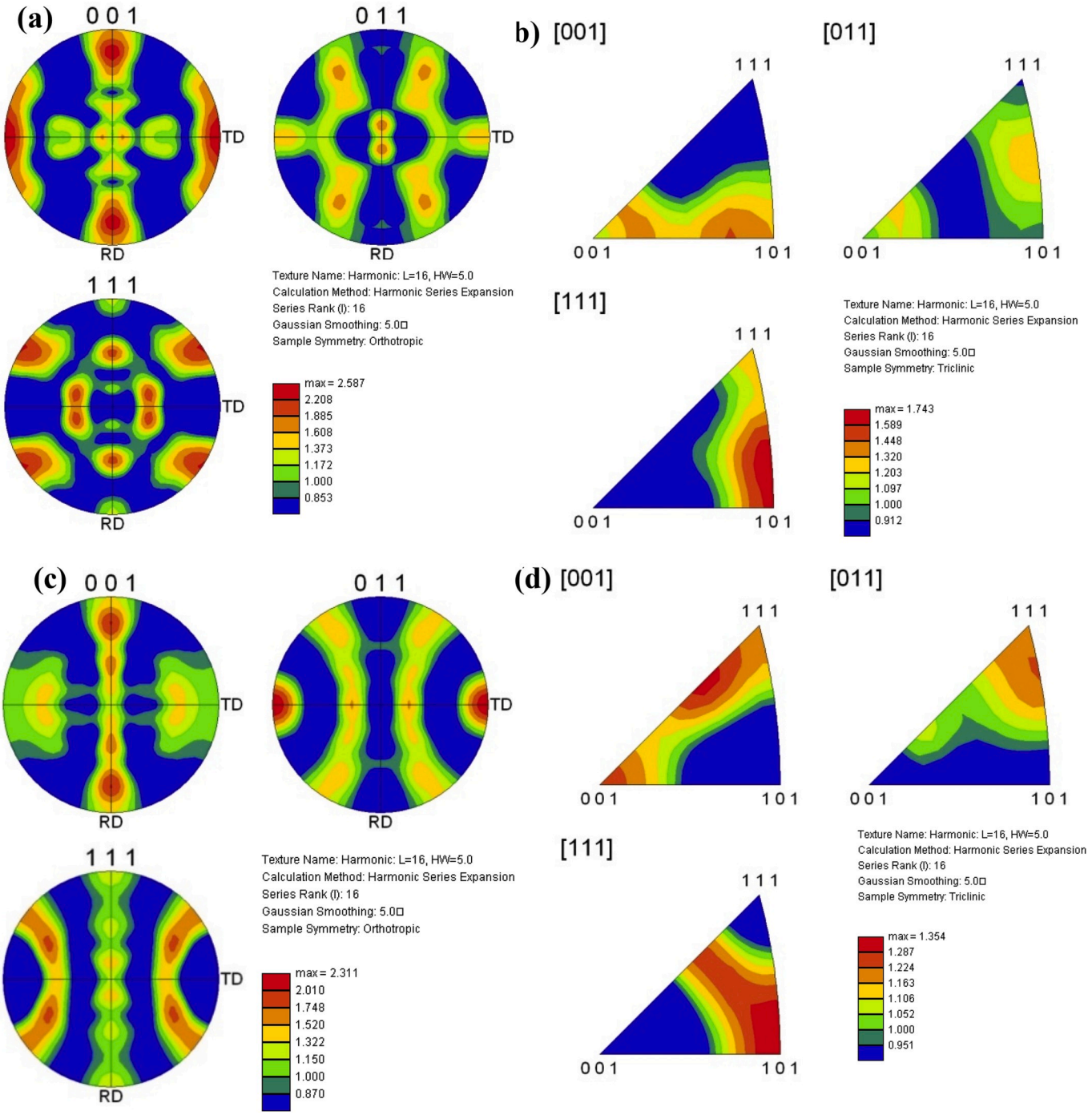

Fig. 4. Pole figures and inverse pole figures of Cu-1.0Co-0.65Si-0.1Ti alloy deformed at 0.01 s^{-1} and different temperatures: (a) and (b) Cu-1.0Co-0.65Si-0.1Ti alloy deformed at 700 °C; (c) and (d) Cu-1.0Co-0.65Si-0.1Ti alloy deformed at 800 °C.

0.1Ti alloy deformed at 0.01 s^{-1} and 800 °C, respectively. It is well known that the work hardening, dynamic recovery and dynamic recrystallization are the three typical characteristics during the hot deformation [11,24,25]. In the early stage of hot deformation, the flow stress increased rapidly due to the work hardening. With the increase of the deformation degree, the effect of dynamic recovery begins to appear, and gradually tends to be balance with the effect of work hardening, that is, the true stress curve tends to level gradually. Moreover, the flow stress decreases at high deformation temperature or low strain rate, which represents the characteristic of the dynamic recovery and dynamic recrystallization. And it can be indicated that the values of the flow stress are mainly affected by the strain rates and deformation temperatures [26,[27]28]. As shown in Fig. 1, the flow stress decreases with the increase of temperature or the decrease of the strain rate. For example, the peak stress of the Cu-1.0Co-0.65Si-0.1Ti alloy decreased from 188 MPa to 155 MPa when the temperature increased from 600 to 700 °C at the strain rate of 0.01 s^{-1}. This is because the average kinetic energy of atoms increases with the increase of temperature, which reduces the critical slip shear force of the deformed alloy, and makes dislocation movement and thermal diffusion more active. Therefore, the increasing of the deformation temperature promotes the nucleation and growth of dynamic recrystallization grains [29]. In addition, the peak stress of the Cu-1.0Co-0.65Si-0.1Ti alloy decreased from 85 MPa to 60 MPa with the strain rate decreased from 0.1 s^{-1} to 0.01 s^{-1}, deformed at

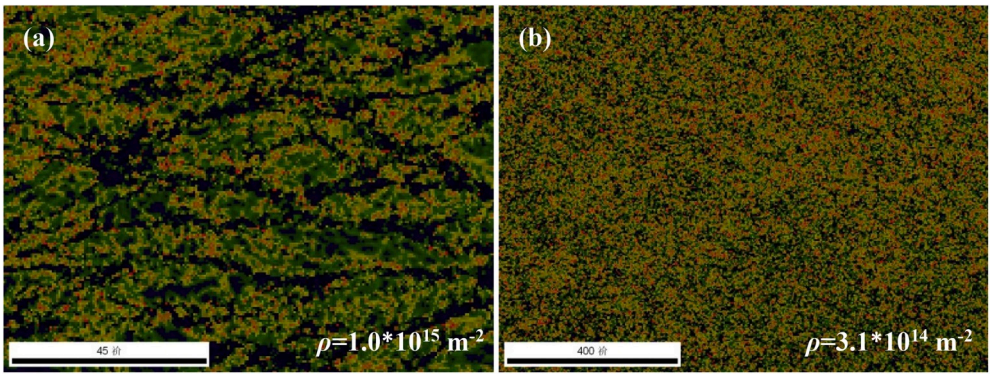

Fig. 5. The Kernel Average Misorientation (KAM) of Cu-1.0Co-0.65Si-0.1Ti alloy: (a) deformed at 700 °C and 0.01 s^{-1}; (b) deformed at 800 °C and 0.01 s^{-1}.

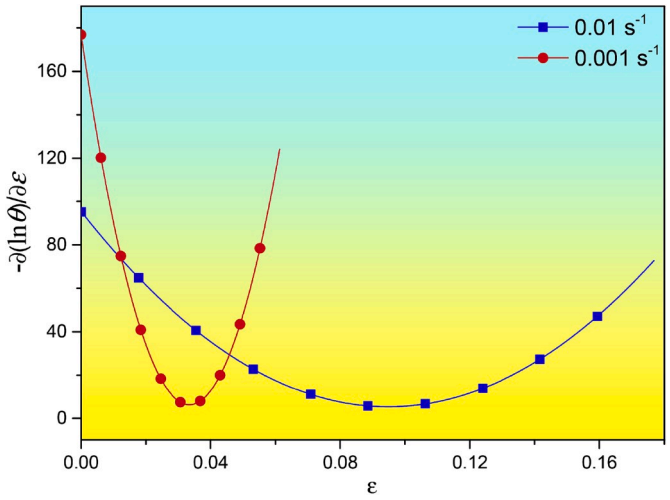

Fig. 6. Strain hardening rate $-\partial(\ln\theta)/\partial\varepsilon$-$\varepsilon$ curve of the Cu-Co-Si-Ti alloy deformed at 800 °C.

800 °C. The reason is that the low strain rate provided sufficient time for dynamic recrystallization, and the degree of dislocation increment was relatively gentle at the low strain rate, so the flow stress of the alloy at lower strain rate was lower.

3.2. Microstructure evolution

The main applications of EBSD are the measurement of orientation and orientation difference, micro-texture analysis, real grain size and so on [30,31]. In order to investigate the microstructure evolution of Cu-1.0Co-0.65Si-0.1Ti alloy during hot deformation, the EBSD images and grain size distributions were shown in Fig. 2. Fig. 2(a) and (c) shows the EBSD images of Cu-1.0Co-0.65Si-0.1Ti alloy deformed at 700 °C, 0.01 s^{-1} and 800 °C, 0.01 s^{-1}, respectively. It can be seen that there are some DRX grains near the deformed grains, which is the characteristics of typical necklace structure [6,32], as shown in Fig. 2(a). And the corresponding grain size distributions are shown in Fig. 2(b). Moreover, the average grain size is 8.5 μm. With the increased of deformation temperature, the necklace structure disappeared gradually, and the deformed grains were replaced by recrystallized grains, i.e. mixed crystal structure appears, which can indicate that the dynamic recrystallization is promoted by the increase of temperature. And the average grain size of Cu-1.0Co-0.65Si-0.1Ti alloy deformed at 800 °C is 14.3 μm, as shown in Fig. 2(d).

Fig. 3 shows the EBSD orientation maps and misorientation angles distributions of Cu-1.0Co-0.65Si-0.1Ti alloy deformed at 700 °C, 0.01 s^{-1} and 800 °C, 0.01 s^{-1}, respectively. As shown in Fig. 3(b) and (d), the distribution of misorientation angles is generally consistent, showing a considerable concentration at the low misorientation angles, which is related to the stored dislocation [33]. There are a great deal of deformed grains and low angle grain boundaries (LAGBs, misorientation angle<15°) for the Cu-1.0Co-0.65Si-0.1Ti alloy deformed at low temperature, which is illustrated in Fig. 3(a) and (b), resulting in the aggregation of dislocations in the deformed grain boundaries and work hardening regions. With the increasing of deformation temperature, the dynamic recrystallization is promoted and the amount of DRX grains is increased, as illustrated in Fig. 3(b). Moreover, the percent of HAGBs increases from 31.4% to 37.0% with the deformation temperature increasing from 700 °C to 800 °C, which can indicate that the enhancement of the dynamic recrystallization and the increased of temperature can swallow up the stored dislocation [34,35]. Therefore, it can be inferred that the increasing of HAGBs means the decreasing of stored dislocation density and the enhancement of dynamic recrystallization.

In order to investigate the texture evolution of Cu-1.0Co-0.65Si-0.1Ti alloy during the hot deformation, the pole figures and inverse pole figures are illustrated in Fig. 4. The common recrystallization textures in fcc metals are the {011} <100> Goss texture, {112} <111> copper texture, {111} <211> R texture, {001} <100> cubic texture and {011} <211> brass texture [36,37]. Fig. 4 shows the pole figures and inverse pole figures of Cu-1.0Co-0.65Si-0.1Ti alloy deformed at 700 °C, 0.01 s^{-1} and 800 °C, 0.01 s^{-1}, respectively. The {011} <100> Goss texture was confirmed, as illustrated in Fig. 4(a) and (b). Moreover, the texture strength of pole figure and inverse pole figure was 2.5 and 1.7, respectively, deformed at 700 °C, 0.01 s^{-1}. With the increasing of deformation temperature, the dynamic recrystallization is promoted. And the {011} <100> Goss texture was gradually substituted by the {112} <111> copper texture, which was shown in Fig. 4(c) and (d). And the corresponding the texture strength of pole figure and inverse pole figure was 2.3 and 1.3, respectively. It can be seen that the texture strength is decreased and the dynamic recrystallization is promoted with the increasing of deformation temperature. The reason is that the process of dynamic recrystallization eliminates the preferred orientation of some deformed grains. In other words, it can infer whether the dynamic recrystallization is promoted or not from the change of texture strength. In addition, the decrease of texture strength corresponds to the decrease of stress-strain curve with the temperature increasing from 700 °C to 800 °C. As illustrated in Wang et al. [12], it investigated that the micro-hardness of Cu-Mg alloys were decreased with the increasing of deformation temperature. Zhao et al. [38] investigated the hot deformation behavior and microstructure evolution of Ti-5Al-5V-5Mo-3Cr alloys prepared by powder metallurgy and ingot metallurgy approaches, and found that the decrease of texture strength corresponds to the decrease of temperature region suitable for hot working. Heidarzadeh et al. [39] analyzed that the yield strength of the copper alloy was decreased with the decrease of texture strength, which can be also

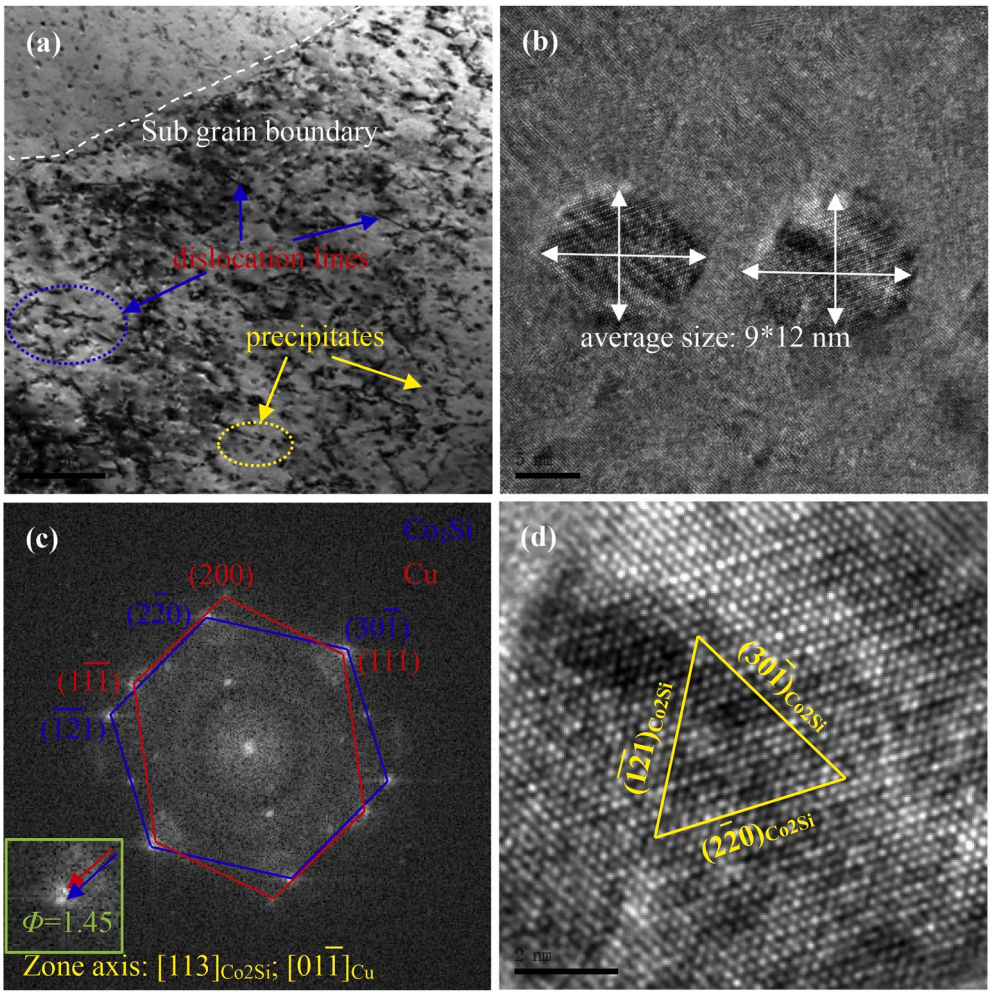

Fig. 7. Microstructure of Cu-1.0Co-0.65Si-0.1Ti alloy deformed at 0.01 s^{-1} and 700 °C: (a) bright field TEM image; (b) HRTEM; (c) FFT of (b); (d) IFFT of (c).

Table 2
Zone axis of the precipitate for beam direction of $[110]_{Cu}$, $[111]_{Cu}$, $[112]_{Cu}$[49].

	Variant	$[110]_{Cu}$	$[111]_{Cu}$	$[112]_{Cu}$
P4	$[101]_{Cu}\|\|[100]_{\delta}$, $(111)_{Cu}\|\|(021)_{\delta}$	$[0.362\ \overline{0.494}\ \overline{0.988}]_{\delta}$	$[0.724\ 0.018\ \overline{0.971}]_{\delta}$	$[1.086\ 0.530\ \overline{0.954}]_{\delta}$

obtained by Haase et al. [36]. On the above analysis, the texture evolution and texture strength are also the parameters to reflect the hot working properties of alloys during hot deformation.

3.3. Dislocation density

The migration of grain boundaries plays an important role in the hot deformation and the migration of grain boundaries is associated with the dislocations near the grain boundaries [40]. Therefore, it is significant to investigate the dislocation density near the grain boundaries of Cu-1.0Co-0.65Si-0.1Ti alloy. The geometrically necessary dislocation (GND) density is related to the local misorientation, which can be represented as [41,42]:

$$\rho^{GND} = 2\theta/\mu b \quad (1)$$

Where, ρ^{GND} is the geometrically necessary dislocation (m^{-2}); θ is the average local misorientation (rad), which is defined the critical value of the average local misorientation as 3°. The misorientation angle larger than this value is excluded in the local misorientation calculation since it is caused by the grain boundaries, not by the GND accumulation. μ is the step size in the scanning and b is the Burger's vector (2.55 nm) [15].

Fig. 5 shows the Kernel Average Misorientation (KAM) of Cu-1.0Co-0.65Si-0.1Ti alloy deformed at 700 °C, 0.01 s^{-1} and 800 °C, 0.01 s^{-1}, respectively. It can be seen that the geometrically necessary dislocation (GND) of Cu-1.0Co-0.65Si-0.1Ti alloy is 1.0×10^{15} m^{-2} and 3.1×10^{14} m^{-2}, respectively. In addition, the GND decreased with the increased of temperature, which indicate that the enhancement of dynamic recrystallization can sacrifice the dislocation.

4. Discussion

4.1. Critical strain

As the name suggesting, the critical strain is the strain at the beginning of dynamic recrystallization. Moreover, the dynamic recovery and dynamic recrystallization are related to the critical strain. H. Mirzadeh et al. [43] investigated that it was inadequate to just judge the dynamic recovery and dynamic recrystallization according to the shape of flow stress curve during the hot deformation of 17-4 PH stainless steel. The analysis of critical strain can accurately determine the initiation

dynamic recovery or dynamic recrystallization [44]. Therefore, it is very important to determine the starting point of dynamic recrystallization of the alloy under various deformation conditions. However, the critical strain cannot be directly determined by the flow stress curve, which can be calculated by the equation of work hardening rate defined by Poliak et al. [4547[46]]. Fig. 6 shows the strain hardening rate $-\partial(\ln\theta)/\partial\varepsilon$-$\varepsilon$ curves of the Cu-Co-Si-Ti alloy deformed at 0.01 s^{-1}, 800 °C and 0.001 s^{-1}, 800 °C. The inflection point of the curves is the starting point of dynamic recrystallization and the inflection point is 0.089 and 0.035 (critical strain), respectively. It can be seen that the decreasing of strain rate reduces the critical strain value, which means that the decreasing of strain rate promotes dynamic recrystallization. Therefore, it can be inferred that the increasing of deformation temperature or decreasing of strain rate can reduce the critical strain and promote the dynamic recrystallization. The same conclusion can be obtained by H. Mirzadeh et al. [48], which investigated the hot deformation behavior of a medium carbon microalloyed steel.

4.2. Precipitates

Fig. 7 shows the TEM micrographs of Cu-1.0Co-0.65Si-0.1Ti alloy deformed at 0.01 s^{-1} and 700 °C. It can be seen that there are a lot of dislocation lines and precipitates in the grains. And the precipitates have a plate-like shape, which have an average size of 12 nm in length and 9 nm in width. Fig. 7(c) and (d) shows the Fast Fourier Transform (FFT) pattern and inverse Fast Fourier Transform (IFFT) pattern corresponding to the HRTEM in Fig. 7(b), respectively. And the precipitate was determined to Co_2Si according the diffraction spot. In addition, the zone axis of Cu and Co_2Si is $[01\bar{1}]_{Cu}$ and $[113]_{Co2Si}$, respectively. It is worth noting that the $(\bar{1}\bar{1}\bar{1})_{Cu}$ is not parallel to the $(\bar{3}01)_{Co2Si}$, but has an angle difference of 1.45°, which is similar with the calculation result (P4) of Table 2 in Yi and Jia et al. [49]. From the definition of diffraction spots, the diffractive spots of Co_2Si after the Fast Fourier Transform (FFT) are clear. However, the diffractive spots of Cu after the Fast Fourier Transform (FFT) are not clear. The reason is that the observation direction of the precipitate is strictly <113>, but the observation direction of copper matrix is not strictly <110>. As illustrated in Fig. 7(d), there are the lattice arrangement directions of $(2\bar{2}0)_{Co2Si}$, $(\bar{1}21)_{Co2Si}$ and $(30\bar{1})_{Co2Si}$.

5. Conclusions

The Cu-1.0Co-0.65Si-0.1Ti alloy was obtained by vacuum melting, and then the hot deformation experiment was carried out by using the Gleeble-1500 simulator at 0.001–10 s^{-1} strain rates and 500–900 °C deformation temperatures, respectively. The microstructure evolution of Cu-1.0Co-0.65Si-0.1Ti alloy was discussed. Several conclusions can be drawn as follows:

(1) With the increasing of deformation temperature, the dynamic recrystallization is promoted and the texture of Cu-1.0Co-0.65Si-0.1Ti alloy transformed from {011} <100> Goss texture to {112} <111> copper texture. Moreover, the precipitate was determined to Co_2Si.
(2) The geometrically necessary dislocation (GND) density was obtained by the Kernel Average Misorientation (KAM). And the GND density decreased with the increased of temperature.
(3) The critical strain of Cu-Co-Si-Ti alloy deformed at 0.01 s^{-1},800 °C and 0.001 s^{-1},800 °C was 0.089 and 0.035, respectively. And it can be inferred that the increasing of deformation temperature or decreasing of strain rate can reduce the critical strain and promote the dynamic recrystallization.

Declaration of competing interest

The authors declare that they have no known competing financial interests or personal relationships that could have appeared to influence the work reported in this paper.

Acknowledgments

This work was supported by the Open Cooperation Project of Science and Technology of the Henan Province (182106000018), Henan University Scientific and Technological Innovation Talent Support Program (18HASTIT024) and the National Natural Science Foundation of China (U1704143).

References

[1] Y. Zhang, B.H. Tian, P. Liu, High temperature deformation behavior and microstructure preparation of Cu-Ni-Si-P alloy, Mater. Sci. Forum 704–705 (2012) 135–140.
[2] A. Meng, J.F. Nie, K. Wei, H.J. Kang, Z.J. Liu, Y.H. Zhao, Optimization of strength, ductility and electrical conductivity of a Cu-Cr-Zr alloy by cold rolling and aging treatment, Vacuum 167 (2019) 329–335.
[3] Z.L. Zhao, Z. Xiao, Z. Li, W.T. Qiu, H.Y. Jiang, Q. Lei, Z.R. Liu, Y.B. Jiang, S. J. Zhang, Microstructure and properties of a Cu-Ni-Si-Co-Cr alloy with high strength and high conductivity, Mater. Sci. Eng., A 759 (2019) 396–403.
[4] W. Tian, L.M. Bi, F.C. Ma, J.D. Du, Effect of Zr on as-cast microstructure and properties of Cu-Cr alloy, Vacuum 149 (2018) 238–247.
[5] K.M. Liu, D.P. Lu, H.T. Zhou, Z.B. Chen, A. Atrens, L. Lu, Influence of a high magnetic field on the microstructure and properties of a Cu-Fe-Ag in situ composite, Mater. Sci. Eng., A 584 (2013) 114–120.
[6] K.M. Liu, Z.Y. Jiang, J.W. Zhao, J. Zou, Z.B. Chen, D.P. Lu, Effect of directional solidification rate on the microstructure and properties of deformation-processed Cu-7Cr-0.1Ag in situ composites, J. Alloys Compd. 612 (2014) 221–226.
[7] B.J. Wang, Y. Zhang, B.H. Tian, J.C. An, Alex A. Volinsky, H.L. Sun, Y. Liu, K. X. Song, Effects of Ce addition on the Cu-Mg-Fe alloy hot deformation behavior, Vacuum 155 (2018) 594–603.
[8] Y. Zhang, H.L. Sun, Alex A. Volinsky, B.H. Tian, K.X. Song, B.J. Wang, Y. Liu, Hot workability and constitutive model of the Cu-Zr-Nd alloy, Vacuum 146 (2017) 35–43.
[9] X.L. Guo, Z. Xiao, W.T. Qiu, Z. Li, Z.Q. Zhao, X. Wang, Y.B. Jiang, Microstructure and properties of Cu-Cr-Nb alloy with high strength, high electrical conductivity and good softening resistance performance at elevated temperature, Mater. Sci. Eng., A 749 (2019) 281–290.
[10] B.M. Luo, D.X. Li, C. Zhao, Z. Wang, Z.Q. Luo, W.W. Zhang, A low Sn content Cu-Ni-Sn alloy with high strength and good ductility, Mater. Sci. Eng., A 746 (2019) 154–161.
[11] K.M. Liu, Z.Y. Jiang, H.T. Zhou, D.P. Lu, A. Atrens, Y.L. Yang, Effect of heat treatment on the microstructure and properties of deformation-processed Cu-7Cr in situ composites, J. Mater. Eng. Perform. 24 (11) (2015) 4340–4345.
[12] B.J. Wang, Y. Zhang, B.H. Tian, V. Yakubov, J.C. An, Alex A. Volinsky, Y. Liu, K. X. Song, L.H. Li, M. Fu, Effects of Ce and Y addition on microstructure evolution and precipitation of Cu-Mg alloy hot deformation, J. Alloys Compd. 781 (2019) 118–130.
[13] A.H. Huang, Y.F. Wang, M.S. Wang, L.Y. Song, Y.S. Li, L. Gao, C.X. Huang, Y. T. Zhu, Optimizing the strength, ductility and electrical conductivity of a Cu-Cr-Zr alloy by rotary swaging and aging treatment, Mater. Sci. Eng., A 746 (2019) 211–216.
[14] J.H. Yuan, L.K. Gong, W.Q. Zhang, B. Zhang, H.G. Wei, X.P. Xiao, H. Wang, B. Yang, Work softening behavior of Cu-Cr-Ti-Si alloy during cold deformation, J Mater. Res. Technol. 8 (2) (2019) 1964–1970.
[15] Y.F. Geng, X. Li, H.L. Zhou, Y. Zhang, Y.L. Jia, B.H. Tian, Y. Liu, Alex A. Volinsky, X.H. Zhang, K.X. Song, G.X. Wang, L.H. Li, J.R. Hou, Effect of Ti addition on microstructure evolution and precipitation in Cu-Co-Si alloy during hot deformation, J. Alloys Compd. 821 (2020) 153518.
[16] Y. Zhang, Alex A. Volinsky, Hai T. Tran, Z. Chai, P. Liu, B.H. Tian, Y. Liu, Aging behavior and precipitates analysis of the Cu-Cr-Zr-Ce alloy, Mater. Sci. Eng., A 650 (2016) 248–253.
[17] J. Li, G.J. Huang, X.J. Mi, L.J. Peng, H.F. Xie, Y.L. Kang, Microstructure evolution and properties of a quaternary Cu-Ni-Co-Si alloy with high strength and conductivity, Mater. Sci. Eng. 766 (2019) 138390.
[18] J.Z. Huang, Z. Xiao, J. Dai, Z. Li, H.Y. Jiang, W. Wang, X.X. Zhang, Microstructure and properties of a novel Cu-Ni-Co-Si-Mg alloy with super-high strength and conductivity, Mater. Sci. Eng., A 744 (2019) 754–763.
[19] R. Zhang, X.B. He, Z. Chen, X.H. Qu, Influence of Ti content on the microstructure and properties of graphite flake/Cu-Ti composites fabricated by vacuum hot pressing, Vacuum 141 (2017) 265–271.
[20] C. Zhao, Z. Wang, D.X. Li, D.Q. Pan, B.M. Lou, Z.Q. Luo, W.W. Zhang, Optimization of strength and ductility in an as-extruded Cu-15Ni-8Sn alloy by the additions of Si and Ti, J. Alloys Compd. 823 (2020) 153759.

[21] K.M. Liu, Z.Y. Jiang, J.W. Zhao, J. Zou, L. Lu, D.P. Lu, Thermal stability and properties of deformation-processed Cu-Fe in situ composites, Metall. Mater. Trans. 46 (5) (2015) 2255–2261.
[22] K.M. Liu, Z.K. Huang, X.W. Zhang, D.P. Lu, A. Atrens, H.T. Zhou, Y. Yin, J.M. Yu, W. Guo, Influence of Ag micro-alloying on the thermal stability and ageing characteristics of a Cu-14Fe in-situ composite, Mater. Sci. Eng., A 673 (2016) 1–7.
[23] Q. Lei, S.Y. Li, J.L. Zhu, Z. Xiao, F.F. Zhang, Z. Li, Microstructural evolution, phase transition, and physics properties of a high strength Cu-Ni-Si-Al alloy, Mater. Char. 147 (2019) 315–323.
[24] C. Roucoules, M. Pietrzyk, P.D. Hodgson, Analysis of work hardening and recrystallization during the hot working of steel using a statistically based internal variable model, Mater. Sci. Eng. 339 (2003) 1–9.
[25] Y.Q. Ning, X. Luo, H.Q. Liang, H.Z. Guo, J.L. Zhang, K. Tan, Competition between dynamic recovery and recrystallization during hot deformation for TC18 titanium alloy, Mater. Sci. Eng. 635 (2015) 77–85.
[26] Z.Y. Dong, S.G. Jia, P.F. Zhao, M. Deng, K.X. Song, Hot deformation behavior of Cu-0.6Cr-0.03Zr alloy during compression at elevated temperatures, Mater. Sci. Eng. 570 (2013) 87–91.
[27] G.L. Ji, G. Yang, L. Li, Q. Li, Modeling constitutive relationship of Cu-0.4 Mg alloy during hot deformation, J. Mater. Eng. Perform. 23 (2014) 1770–1779.
[28] W.L. Cheng, Y. Bai, S.C. Ma, L.F. Wang, H.X. Wang, H. Yu, Hot deformation behavior and workability characteristic of a fine-grained Mg-8Sn-2Zn-2Al alloy with processing map, J. Mater. Sci. Technol. 35 (2019) 1198–1209.
[29] Y. Liu, S. Shao, K.M. Liu, X.J. Yang, D.P. Lu, Microstructure refinement mechanism of Cu-7Cr in situ composites with trace Ag, Mater. Sci. Eng., A 531 (2012) 141–146.
[30] R. Mishnev, I. Shakhova, A. Belyakov, R. Kaibyshev, Deformation microstructures, strengthening mechanisms, and electrical conductivity in a Cu-Cr-Zr alloy, Mater. Sci. Eng., A 629 (2015) 29–40.
[31] F. Bittner, S. Yin, A. Kauffmann, J. Freudenberger, H. Klauß, G. Korpala, R. Kawalla, W. Schillinger, L. Schultz, Dynamic recrystallisation and precipitation behavior of high strength and highly conducting Cu-Ag-Zr alloys, Mater. Sci. Eng., A 597 (2014) 139–147.
[32] J. Liu, X.H. Wang, J.T. Liu, Y.F. Liu, H.Y. Li, C. Wang, Hot deformation and dynamic recrystallization behavior of Cu-3Ti-3Ni-0.5Si alloy, J. Alloys Compd. 782 (2019) 224–234.
[33] W.J. He, A. Chapuis, X. Chen, Q. Liu, Effect of loading direction on the deformation and annealing behavior of a zirconium alloy, Mater. Sci. Eng., A 734 (2018) 364–373.
[34] S.H. Liu, Q.L. Pan, M.J. Li, X.D. Wang, X. He, X.Y. Li, Z.W. Peng, J.P. Lai, Microstructure evolution and physical-based diffusion constitutive analysis of Al-Mg-Si alloy during hot deformation, Mater. Des. 184 (2019) 108181.
[35] G.A. He, Y.F. Zhao, B. Gan, X.F. Sheng, Y. Liu, L.M. Tan, Mechanism of grain refinement in an equiatomic medium-entropy alloy CrCoNi during hot deformation, J. Alloys Compd. 815 (2020) 152382.
[36] C. Haase, L.A. Barrales-Mora, Influence of deformation and annealing twinning on the microstructure and texture evolution of face-centered cubic high-entropy alloys, Acta Mater. 150 (2018) 88–103.
[37] Q. Lei, Z. Li, W.P. Hu, Y. Liu, C.L. Meng, B. Derby, W. Zhang, Microstructure evolution and hardness of an ultra-high strength Cu-Ni-Si alloy during thermo-mechanical processing, J. Mater. Eng. Perform. 25 (2016) 2615–2625.
[38] Q.Y. Zhao, F. Yang, R. Torrens, L. Bolzoni, Comparison of hot deformation behaviour and microstructural evolution for Ti-5Al-5V-5Mo-3Cr alloys prepared by powder metallurgy and ingot metallurgy approaches, Mater. Des. 169 (2019) 107682.
[39] A. Heidarzadeh, T. Saeid, V. Klemmc, A. Chabok, Y.T. Pei, Effect of stacking fault energy on the restoration mechanisms and mechanical properties of friction stir welded copper alloys, Mater. Des. 162 (2019) 185–197.
[40] K.M. Liu, Z.X. Wang, Z.Y. Jiang, A. Atrens, Z.K. Huang, W. Guo, X.W. Zhang, J. M. Yu, Q.G. Lu, D.P. Lu, Cu-7Cr-0.1Ag microcomposites optimized for high strength and high conductivity, J. Mater. Eng. Perform. 27 (3) (2018) 933–938.
[41] Y.S. Wu, X.Z. Qin, C.S. Wang, L.Z. Zhou, Influence of phosphorus on hot deformation microstructure of a Ni-Fe-Cr based alloy, Mater. Sci. Eng., A 768 (2019) 138454.
[42] Y.S. Wu, Z. Liu, X.Z. Qin, C.S. Wang, L.Z. Zhou, Effect of initial state on hot deformation and dynamic recrystallization of Ni-Fe based alloy GH984G for steam boiler applications, J. Alloys Compd. 795 (2019) 370–384.
[43] H. Mirzadeh, A. Najafifizadeh, Prediction of the critical conditions for initiation of dynamic recrystallization, Mater. Des. 31 (2010) 1174–1179.
[44] S. Saadatkia, H. Mirzadeh, J.M. Cabrera, Hot deformation behavior, dynamic recrystallization, and physically-based constitutive modeling of plain carbon steels, Mater. Sci. Eng., A 636 (2015) 196–202.
[45] E.I. Poliakt, J.J. Jonass, A one-parameter approach to determining the critical conditions for the initiation OF dynamic recrystallization, Acta Mater. 44 (1996) 127–136.
[46] A. Manonukul, F.P.E. Dunne, Initiation OF dynamic recrystallization under inhomogeneous stress states IN pure copper, Acta Mater. 47 (1999) 4339–4354.
[47] E.I. Poliak, J.J. Jonas, Initiation of dynamic recrystallization in constant strain rate hot deformation, ISIJ Int. 43 (2003) 684–691.
[48] H. Mirzadeh, J.M. Cabrera, J.M. Prado, A. Najafizadeh, Hot deformation behavior of a medium carbon microalloyed steel, Mater. Sci. Eng., A 528 (2011) 3876–3882.
[49] J. Yi, Y.L. Jia, Y.Y. Zhao, Z. Xiao, K.J. He, Q. Wang, M.P. Wang, Z. Li, Precipitation behavior of Cu-3.0Ni-0.72Si alloy, Acta Mater. 166 (2019) 261–270.